Classical dynamics of resonantly modulated large-spin systems

C. Hicke and M. I. Dykman
Department of Physics and Astronomy, Michigan State University, East Lansing, Michigan 48824, USA
(Received 15 February 2008; revised manuscript received 2 May 2008; published 1 July 2008)

We study the classical dynamics of resonantly modulated large-spin systems in a strong magnetic field, where the Zeeman energy exceeds the anisotropy energy. We show that these systems have special symmetry. It leads to characteristic nonlinear effects. They include abrupt switching between magnetization branches with varying modulating field without hysteresis and a specific pattern of switching in the presence of multistability and hysteresis. Along with steady forced vibrations, the transverse spin components can display incoherent vibrations at a combination of the Larmor frequency and a smaller frequency determined by the anisotropy constant. The analysis is based on a microscopic theory that takes into account relaxation mechanisms important for single-molecule magnets and other large-spin systems. We find how the Landau–Lifshitz model should be modified in order to describe the classical spin dynamics. The occurrence of incoherent oscillations depends on the interrelation between the relaxation parameters.

DOI: 10.1103/PhysRevB.78.024401 PACS number(s): 75.50.Xx, 76.20.+q, 76.50.+g, 03.65.Sq

I. INTRODUCTION

Large-spin systems have a finite but comparatively large number of quantum states. Therefore, a single system can be used to study a broad range of phenomena from purely quantum to classical where the spin behaves like a top. One of the interesting features of large-spin systems is that, in a strong static magnetic field, their energy levels become almost equidistant, with level spacing close to $\hbar\omega_0$, where ω_0 is the Larmor frequency. As a result, radiation at frequency $\approx\omega_0$ is resonant simultaneously for many interlevel transitions. This leads to new quantum and classical nonlinear resonant effects.

An important class of large-spin systems is single-molecule magnets (SMMs). SMMs display an extremely rich behavior and have been attracting much attention in recent years. A variety of SMMs has already been discovered and investigated (see Refs. 1–3 for a review) and new systems are being found.[4,5] Another example of large-spin systems is provided by large nuclear spins, the interest in which has renewed in view of their possible use in quantum computing.[6]

In this paper, we study the dynamics of large-spin systems, $S\gg 1$, in the classical limit. We assume that the system is in a strong static magnetic field along the easy magnetization axis and the Zeeman energy is much larger than the anisotropy energy. Then, for a small relaxation rate, the response to even a moderately small transverse resonant field can show hysteresis.

In the absence of relaxation, the quantum dynamics of a resonantly modulated spin has special features, one of which is an antiresonance of the response that accompanies anticrossing of quasienergy levels.[7] Quantum spin dynamics in the rotating frame bears also on the dynamics of the Lipkin–Meshkov–Glick model.[8–11]

One may expect that the features of the coherent quantum dynamics should have counterparts in the classical spin dynamics in the presence of dissipation. As we show, this is indeed the case. The system displays an unusual behavior in a certain range of modulation parameters. This behavior is due to a special symmetry. It leads to specific features of hysteresis and to discontinuous (in the neglect of fluctuations) switching between different response branches even in the absence of hysteresis.

Classical dynamics of a large-spin system in a resonant field would be expected to have similarities with the dynamics of a modulated magnetic nanoparticle near ferromagnetic resonance. It was understood back in the 1950s (Refs. 12 and 13) that the response near ferromagnetic resonance becomes strongly nonlinear already for a comparatively weak radiation strength due to the magnetization dependence of the effective magnetic field. The resonant response may become multivalued as a function of the modulating field amplitude.[14,15] A detailed analysis of nonlinear magnetization dynamics in uniaxial nanoparticles modulated by a strong circularly polarized periodic field was done recently.[16] These studies as well as many other studies of magnetization dynamics in ferromagnets were based on the phenomenological Landau–Lifshitz–Gilbert equation.

In distinction from ferromagnets, in large-spin systems, relaxation occurs via transitions between discrete spin energy levels with emission, absorption, or inelastic scattering of excitations of a thermal reservoir to which the spin is coupled. Relevant relaxation mechanisms depend on the specific system but as we show, even in the classical limit relaxation is not described, generally, by the Landau–Lifshitz damping. As a result, the classical spin dynamics strongly differs from the dynamics of a magnetic nanoparticle.

The microscopic analysis of relaxation is simplified in the presence of a strong static magnetic field. Here, all spin energy levels are almost equidistant, as mentioned above. Therefore, excitations of the thermal bath emitted, for example, in transitions within different pairs of neighboring levels have almost the same energies. As a consequence, relaxation is described by a small number of constants independent of the form of the weighted with the interaction density of states of the bath. The analysis applies for an arbitrary ratio between the level nonequidistance due to magnetic anisotropy and the level broadening due to relaxation.[17]

We consider three relaxation mechanisms. Two of them correspond to transitions between neighboring and next

neighboring spin levels, with the coupling to bosonic excitations quadratic in the spin operators. Such coupling is important, in particular, for SMMs where energy relaxation is due to phonon scattering. The theory of relaxation of SMMs was developed earlier[18,19] and has been tested experimentally (see Refs. 20 and 21 and papers cited therein). We also consider coupling to a bosonic bath linear in spin operators. It leads to relaxation that in the classical limit has the form of the Landau–Lifshitz damping provided the modulation field is weak compared to the static field.

We analyze the spin dynamics in the rotating wave approximation (RWA). Since the typical duration of scattering events that lead to spin relaxation is often $\sim\omega_0^{-1}$, in the RWA they appear instantaneous. The operator that describes relaxation has a simple functional form, with no retardation in the "slow" time. This is advantageous for studying the classical limit and allows us to obtain analytical results.

In the classical limit, a spin is characterized by two dynamical variables, for example, azimuthal and polar angles. In the RWA, they satisfy autonomous equations of motion, i.e., the coefficients in these equations do not depend on time. A two-variable nonlinear dissipative system can have both stationary and periodicity.[22] As we show, such states indeed emerge for a resonantly modulated spin. The occurrence of stationary and periodic states was predicted also for a strongly and, in general, nonresonantly modulated magnetic nanoparticle with Landau–Lifshitz damping.[16]

For a spin, the occurrence of periodic states in the rotating frame critically depends on the interrelation between the relaxation parameters. In particular, we show that these states do not emerge for a comparatively weak resonant modulation if the microscopic relaxation is of the same form as the Landau–Lifshitz damping. Moreover, quantum fluctuations lead to phase diffusion, which results in the decay of periodicity in the rotating frame, making the corresponding vibrations incoherent.

The paper is organized as follows. In Sec. II, we introduce a model of the spin and its interaction with a thermal bath and derive the quantum kinetic equation with account taken of different relaxation mechanisms. In Sec. III, we obtain classical equations of motion and discuss the symmetry of the system. We find analytically, for weak damping, the positions of the bifurcation curves where the number of stationary states in the rotating frame changes (saddle-node bifurcations) and where periodic states are split off from stationary states (Hopf bifurcations). Section IV describes the specific and, perhaps, most unusual feature of the system, the occurrence of Hamiltonian-like dynamics in the presence of dissipation. In Sec. V, spin dynamics and hysteresis are described for the relation between relaxation parameters where the system does not have periodic states in the rotating frame. In Sec. VI, we consider the opposite case. The onset of periodic states and their stability are analyzed and the features of the hysteresis related to the occurrence of periodic states are studied. Details of the calculations are outlined in the Appendix. Section VII contains concluding remarks.

II. MODEL

We consider a large spin, $S \gg 1$, in a strong stationary magnetic field along the easy axis z. The spin is modulated by a transverse magnetic field with frequency ω_F close to the Larmor frequency ω_0. The Hamiltonian of the spin has the form

$$H_0 = \omega_0 S_z - \frac{1}{2} D S_z^2 - S_x A \cos \omega_F t \quad (\hbar = 1). \tag{1}$$

This Hamiltonian well describes many single-molecule magnets, including Mn_{12} crystals; D characterizes the magnetic anisotropy and A is the modulation amplitude. It also describes a nuclear spin, with D characterizing the quadrupolar coupling energy to an electric field gradient in the crystal with an appropriate symmetry.

We assume that the Zeeman energy levels in the absence of modulation are almost equidistant. We also assume that the resonant modulation is not too strong. These conditions are met provided,

$$|\omega_0 - \omega_F|, DS, A \ll \omega_0. \tag{2}$$

For many SMMs, the inequality $DS \ll \omega_0$ is fairly demanding and requires strong static magnetic fields; for example, $D \approx 0.6$ K for Fe_8, where $S=10$,[3] so that $DS=\omega_0$ for a field ≈ 5 T. On the other hand, for more isotropic SMMs, the anisotropy is much smaller; for example, $D \sim 0.04$ K for Mn_{11}, where $S=13$,[23] and $D \approx 0.04$ K for Fe_{17}, where $S=35/2$ (see Ref. 5) (our definition of D differs by a factor of 2 from the definition used in the literature on SMMs). For large-S nuclei, where D and the magnetic moment are much smaller than in SMMs, condition (2) can often be met by applying a magnetic field of only a few teslas.

The quantum dynamics of an isolated spin with Hamiltonian H_0 [Eq. (1)] was considered earlier.[7] Here, we are interested in the spin dynamics in the presence of dissipation. Different dissipation mechanisms are important for different systems. For SMMs, energy dissipation is due primarily to transitions between spin energy levels accompanied by emission or absorption of phonons. The transitions between both nearest and next nearest spin levels are important.[18,19,24] The corresponding interactions are

$$H_i^{(1)} = \sum\nolimits_k V_k^{(1)} (S_+ S_z + S_z S_+) b_k + \text{H.c.}$$

$$H_i^{(2)} = \sum\nolimits_k V_k^{(2)} S_+^2 b_k + \text{H.c.}, \quad S_\pm = S_x \pm i S_y, \tag{3}$$

where k enumerates phonon modes, b_k is the annihilation operator for the kth mode, and $V_k^{(1)}$ and $V_k^{(2)}$ are the coupling parameters responsible for transitions between nearest and next nearest Zeeman levels. The phonon Hamiltonian is

$$H_{ph} = \sum\nolimits_k \omega_k b_k^+ b_k. \tag{4}$$

A similar interaction Hamiltonian describes the coupling of a nuclear spin to phonons (cf. Ref. 25 and the early work[26,27]).

Along with interaction (3), we will consider the interaction that is linear in the spin operators,

$$H_i^{(3)} = \sum\nolimits_k V_k^{(3)} S_+ b_k + \text{H.c.}. \tag{5}$$

Such interaction is allowed by time-reversal symmetry in the presence of a strong static magnetic field, with the coupling

constants $V_k^{(3)}$ proportional to an odd (e.g., first) power of the field. It can be thought of as arising from phonon-induced modulation of the spin g factor. The interaction $H_i^{(3)}$ [Eq. (5)] is also important for impurity spins in magnetic crystals, in which case b_k is the annihilation operator of a magnon.[28,29]

A. Rotating wave approximation

The dynamics of a periodically modulated spin can be conveniently described in the RWA. To do this, we make a canonical transformation $U(t)=\exp(-i\omega_F S_z t)$. The transformed Hamiltonian H_0 then becomes $\tilde{H}_0=U^\dagger H_0 U - iU^\dagger \dot{U}$,

$$\tilde{H}_0 = -\delta\omega S_z - \frac{1}{2}DS_z^2 - \frac{1}{2}AS_x,$$

$$\delta\omega = \omega_F - \omega_0. \tag{6}$$

Here, we disregarded fast-oscillating terms $\propto A\exp(\pm 2i\omega_F t)$.

The RWA Hamiltonian (6) has the form of a free energy of a magnetic moment in an easy axis ferromagnet, with **S** playing the role of the magnetization and $\delta\omega$ and A giving the components of the effective magnetic field (in energy units) along the z and x axes, respectively. We note that for some types of single-molecule magnets the spin anisotropy energy H_0 along with DS_z^2 has a term $E(S_x^2-S_y^2)$.[3] It leads to a fast-oscillating term in $\tilde{H}_0$, which can be disregarded in the RWA, to first order in E.

It is convenient to change to dimensionless variables and rewrite the Hamiltonian as $\tilde{H}_0=S^2D(\hat{g}+\mu^2/2)$, with

$$\hat{g} = -\frac{1}{2}(s_z+\mu)^2 - fs_x,$$

$$\mathbf{s}=\mathbf{S}/S, \quad \mu=\delta\omega/SD, \quad f=A/2SD. \tag{7}$$

The Hamiltonian $\hat{g}$ describes the dynamics of an isolated spin in "slow" dimensionless time $\tau=SDt$. It gives dimensionless quasienergies of a periodically modulated spin in the RWA. From Eq. (7), the spin dynamics is determined by the two dimensionless parameters, μ and f, which depend on the interrelation between the frequency detuning of the modulating field $\delta\omega$, the anisotropy parameter DS, and the modulation amplitude A. The spin variables $\hat{\mathbf{s}}$ are advantageous for describing large spins since the commutators of their components are $\propto S^{-1}$, which simplifies a transition to the classical limit for $S\gg 1$.

B. Quantum kinetic equation

We will assume that the interaction with phonons (magnons) is weak. Then, under standard conditions the equation of motion for the spin density matrix ρ is Markovian in slow time τ, i.e., on a time scale that largely exceeds ω_F^{-1} and the typical correlation time of phonons (magnons). We will switch to the interaction representation with respect to the Hamiltonian $\omega_F S_z+H_{ph}$. Then, to leading order in the spin to bath coupling, the quantum kinetic equation can be written as

$$S^{-1}\partial_\tau\rho = i[\rho,g] - \hat{\Gamma}^{(1)}\rho - \hat{\Gamma}^{(2)}\rho - \hat{\Gamma}^{(3)}\rho. \tag{8}$$

The operators $\hat{\Gamma}^{(j)}$ describe relaxation due to the interactions $H_i^{(j)}$, with $j=1,2,3$. They can be written schematically as

$$\hat{\Gamma}\rho = \Gamma[(\bar{n}+1)(L^+L\rho - 2L\rho L^+ + \rho L^+L) + \bar{n}(LL^+\rho - 2L^+\rho L + \rho LL^+)]. \tag{9}$$

Here, we have taken into account that all transitions between spin states with emission or absorption of phonons (magnons) involve almost the same energy transfer ΔE, with $\Delta E\approx\omega_F$ for terms $\propto\Gamma^{(1)},\Gamma^{(3)}$ and $\Delta E\approx 2\omega_F$ for the term $\propto\Gamma^{(2)}$. In this sense, the equation for spin relaxation (9) resembles the quantum kinetic equation for a weakly nonlinear oscillator coupled to a bosonic bath;[17] $\bar{n}$ is the Planck number of the emitted and/or absorbed bosons, $\bar{n}=[\exp(\Delta E/kT-1)]^{-1}$. Because of the same transferred energy, different transitions are characterized by the same rate constants, which for the interactions $H_i^{(1)-(3)}$ have the following form in dimensionless time:

$$\Gamma^{(1)} = \pi D^{-1}S^2\sum\nolimits_k |V_k^{(1)}|^2\delta(\omega_F-\omega_k),$$

$$\Gamma^{(2)} = \pi D^{-1}S^2\sum\nolimits_k |V_k^{(2)}|^2\delta(2\omega_F-\omega_k),$$

$$\Gamma^{(3)} = \pi D^{-1}\sum\nolimits_k |V_k^{(3)}|^2\delta(\omega_F-\omega_k). \tag{10}$$

The operators L for the interactions $H_i^{(1)-(3)}$ are

$$L^{(1)} = s_-s_z + s_zs_-, \quad L^{(2)} = s_-^2, \quad L^{(3)} = s_-, \tag{11}$$

where $s_\pm=S_\pm/S$.

It is important to note that, along with dissipation, coupling to phonons (magnons) leads to a polaronic effect of renormalization of the spin energy. A standard analysis shows that renormalization due to $H_i^{(3)}$, to second order in $H_i^{(3)}$, comes to a change of the anisotropy parameter D and the Larmor frequency. A similar change comes from the nonresonant terms $\propto S_+b_k^\dagger$+H.c.. In contrast, renormalization from $H_i^{(1),(2)}$, along with terms $\propto S_z, S_z^2$, leads to terms of higher order in S_z in the spin Hamiltonian, in particular, to terms $\propto S_z^4$. The condition that they are small compared to the anisotropy energy DS_z^2 imposes a constraint on the strength of the coupling $H_i^{(1),(2)}$ [this is not a strong constraint, generally: for example, one can think of coupling to phonons as resulting from phonon-induced modulation of the anisotropy energy[18]]. Respectively, we will assume that the dimensionless decay rates $\Gamma^{(1),(2)}$ are small, $\Gamma^{(1),(2)}\ll 1$. It is not necessary to impose a similar condition on the dimensionless rate $\Gamma^{(3)}$. Still, we will be interested primarily in the spin dynamics in the underdamped regime, where $\Gamma^{(1)-(3)}$ are all small.

III. CLASSICAL MOTION OF THE MODULATED SPIN

The analysis of spin dynamics is significantly simplified in the classical or mean-field limit. Classical equations of

motion for the spin components can be obtained by multiplying Eq. (8) by s_i $(i=x,y,z)$, taking the trace, and decoupling $\mathrm{Tr}(s_{i_1}s_{i_2}\rho)\to s_{i_1}s_{i_2}$. The decoupling should be done after the appropriate commutators are evaluated; for example, $\mathrm{Tr}([s_z,\hat{g}]\rho)\to -ifs_y$. From Eqs. (7), (8), and (11), we obtain

$$\dot{\mathbf{s}} = -\mathbf{s}\times\partial_{\mathbf{s}}g + (\dot{\mathbf{s}})_d, \quad (\dot{\mathbf{s}})_d = \Gamma_d(s_z)\mathbf{s}\times(\mathbf{s}\times\hat{\mathbf{z}}),$$

$$\Gamma_d(s_z) = 2(4\Gamma^{(1)}s_z^2 + 2\Gamma^{(2)}(1-s_z^2) + \Gamma^{(3)}), \tag{12}$$

where $\hat{\mathbf{z}}$ is a unit vector along the z axis, which is the direction of the strong dc magnetic field, and $\dot{\mathbf{s}}\equiv d\mathbf{s}/d\tau$.

We have assumed in Eq. (12) that $S\gg\bar{n}$. Note that in dimensional units, $S=|\mathbf{L}|/\hbar$, where $\mathbf{L}$ is the angular momentum, whereas in the classical temperature limit, $\bar{n}=kT/\hbar\omega_F$ or $kT/2\hbar\omega_F$ depending on the scattering mechanism. Therefore, the condition $S\gg\bar{n}$ imposes a $\hbar$-free limitation on temperature.

Equation (12) is reminiscent of the Landau–Lifshitz equation for magnetization of a ferromagnet. However, in contrast to the Landau–Lifshitz equation a retardation-free equation of motion for a classical spin could be obtained only in the rotating frame, that is, in slow time τ. The term with $\partial_{\mathbf{s}}g$ describes precession of a spin with energy (quasienergy, in the present case) g. The term $(\dot{\mathbf{s}})_d$ describes the effective friction force. It is determined by the instantaneous spin orientation, but its form is different from that of the friction force in the Landau–Lifshitz equation.

We emphasize that Eq. (12) is not phenomenological; it is derived for the microscopic model of coupling to the bath [Eqs. (3) and (5)]. We now consider what would happen if we start from the Landau–Lifshitz equation and switch to the rotating frame using the RWA in the assumption that the resonant driving is comparatively weak, $A\ll\omega_0$ [cf. Eq. (2)]. In this case, one should keep in the expression for the friction force only the leading term in the effective magnetic field, i.e., assume that $\mathbf{H}\|\hat{\mathbf{z}}$. The result would be Eq. (12) with a dissipative term of the same form as the term $\propto\Gamma^{(3)}$ but without dissipative terms that have the structure of the terms $\propto\Gamma^{(1)},\Gamma^{(2)}$. However, these latter terms play a major role for SMMs[18–21] and for phonon scattering by nuclear spins.

As mentioned in Sec. I, the dynamics of a single-domain magnetic nanoparticle in a circularly polarized field was studied using the Landau–Lifshitz–Gilbert equation in a series of papers.[16] It is clear from the above comment that the results of this analysis do not generally describe the resonant behavior of SMMs. Moreover, as shown below, periodic states in the rotating frame predicted in Ref. 16 do not arise in resonantly excited spin systems with the Landau–Lifshitz–Gilbert-type relaxation $\propto\Gamma^{(3)}$.

A. Stationary states in the rotating frame for weak damping

A classical spin is characterized by its azimuthal and polar angles, ϕ and θ, with $s_z=\cos\theta, s_x=\sin\theta\cos\phi, s_y=\sin\theta\sin\phi$. In canonically conjugate variables ϕ, s_z, equations of motion (12) take the form

$$\dot{\phi} = \partial_{s_z}g,$$

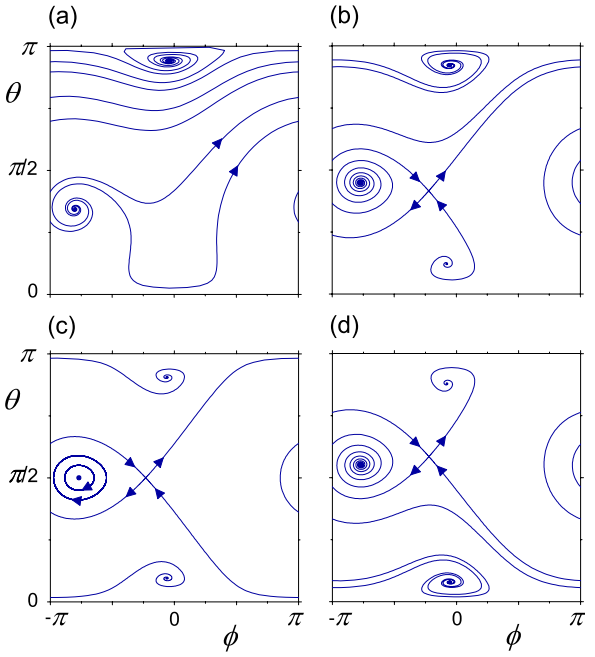

FIG. 1. (Color online) Phase portraits of the spin on (θ,ϕ)-plane $(s_z=\cos\theta)$. The data refer to the scaled decay rates $\Gamma^{(1)}=\Gamma^{(2)}=0$ and $\Gamma^{(3)}=0.1$ and the scaled resonant field amplitude $f=0.3$. In panels (a)–(d), the scaled frequency detuning is $\mu=-0.6$, -0.2, 0, and 0.2, respectively.

$$\dot{s}_z = -\partial_\phi g - \Gamma_d(s_z)(1-s_z^2), \tag{13}$$

where g as a function of s_z,ϕ has the form $g=-(s_z+\mu)^2/2 - f(1-s_z^2)^{1/2}\cos\phi$ [cf. Eq. (7)]. We note that the dissipation term is present only in the equation for $\dot{s}_z$.

In the absence of relaxation, precession of a spin with given g corresponds to moving along orbits on the (ϕ,s_z) plane. The orbits can be either closed or open; in the latter case, ϕ varies by 2π over a period (cf. Fig. 1). There are also stationary states where the spin orientation does not vary in time. Generally, relaxation breaks this structure. If it is weak it makes some of the stationary states asymptotically stable or unstable and can also transform some of the orbits into stable or unstable limit cycles, which correspond to periodic oscillations of s_z and ϕ in the rotating frame. The frequency of these oscillations is determined by the system nonlinearity and is not immediately related to a combination of the modulation frequency and the Larmor frequency, for example.

Since Eq. (13) is written in the rotating frame, its stationary states correspond to the states of forced vibrations of the spin components s_x,s_y at frequency ω_F in the laboratory frame. Periodic states in the rotating frame correspond, in the laboratory frame, to periodic vibrations of s_z and to vibrations of s_x,s_y at combination frequencies equal to ω_F with added and subtracted multiples of the oscillation frequency in the rotating frame (which is small compared to ω_F). In what follows, we keep this correspondence in mind, but the discussion refers entirely to the rotating frame.

The analysis of stability of stationary states is based on linearizing the equations of motion near these states and looking at the corresponding eigenvalues λ_1,λ_2.[22] In the ab-

sence of damping, the stationary states are either hyperbolic points (saddles) with real $\lambda_{1,2}$ or elliptic points (centers) with imaginary $\lambda_{1,2}$. From Eq. (13), a fixed point is hyperbolic if $\lambda_1\lambda_2=\mathcal{D}<0$, where

$$\mathcal{D}=\partial_\phi^2 g\partial_{s_z}^2 g-(\partial_\phi\partial_{s_z}g)^2 \tag{14}$$

(the derivatives are calculated at the stationary state). On the other hand, if $\mathcal{D}>0$ the stationary state corresponds to an elliptic point, orbits $g=$const are circling around it.

For weak damping, hyperbolic points remain hyperbolic. On the other hand, a center becomes asymptotically stable (an attractor) or unstable (a repeller) for $\mathcal{T}<0$ or $\mathcal{T}>0$, respectively. Here, $\mathcal{T}=-\partial[\Gamma_d(s_z)(1-s_z^2)]/\partial s_z$, or in explicit form

$$\mathcal{T}=-4s_z[4\Gamma^{(1)}(1-2s_z^2)-4\Gamma^{(2)}(1-s_z^2)-\Gamma^{(3)}], \tag{15}$$

where s_z is taken for the appropriate center; $\lambda_1+\lambda_2=\mathcal{T}$. The sign of $\mathcal{T}$ determines stability of a stationary state also where dissipation is not small.

The quasienergy g has symmetry properties that the change $f\to -f$ can be accounted for by replacing $\phi\to\phi+\pi$ and $s_z\to s_z$. This replacement preserves the form of equations of motion (13) also in the presence of damping. Therefore, in what follows, we will concentrate on the range $f\geq 0$. On the other hand, the change $\mu\to-\mu$ would not change g if we simultaneously replace $\phi\to\phi$ and $s_z\to -s_z$. In equations of motion, one should additionally change $\tau\to-\tau$. Therefore, if for $\mu=\mu^{(0)}<0$, the system has an attractor located at a given $(\phi^{(0)},s_z^{(0)})$, then for $\mu=-\mu_0$, it has a repeller located at $\phi^{(0)},-s_z^{(0)}$. This behavior is illustrated in Fig. 1, where Figs. 1(b) and 1(d) refer to the opposite values of μ.

B. Saddle-node bifurcations

The function $g(\mathbf{s})$ has a form of the free energy of a magnetic moment of an easy axis ferromagnet, as mentioned earlier, with μ and f corresponding to the components of the magnetic field along and transverse to the easy axis, respectively. It is well known that g may have either two or four extreme points, where $\partial g/\partial s_z=\partial g/\partial\phi=0$. The region where there are four extrema lies inside the Stoner–Wohlfarth astroid[30] $|f|^{2/3}+|\mu|^{2/3}=1$ on the plane of the dimensionless parameters μ and f [see Fig. 2(a)]. The extrema of g outside the astroid are a minimum and a maximum, whereas inside the astroid, g additionally has a saddle and another minimum or maximum. All of them lie at $\phi=0$ or $\phi=\pi$.

In the presence of weak damping, the minima and maxima of g become stable or unstable stationary states. We note that there are no reasons to expect that the stable states lie at the minima of g because g is not an energy but a quasienergy of the spin. The number of stable and/or unstable stationary states changes on the saddle-node bifurcation curve on the (f,μ) plane. The condition that two stationary states merge[22] has the form

$$\mathcal{D}+\mathcal{T}\partial_\phi\partial_{s_z}g=0. \tag{16}$$

For weak damping, a part of the curve given by this equation is close to the astroid. On the astroid, $s_z=-\mathrm{sgn}(\mu)|\mu|^{1/3}$.

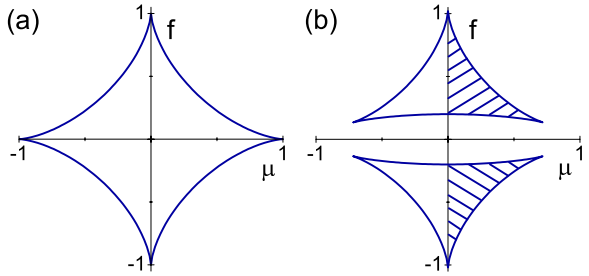

FIG. 2. (Color online) Saddle-node bifurcation lines. Panel (a): zero-damping limit; the lines have the form of the Stoner–Wolfarth astroid in the variables of reduced amplitude f and frequency detuning μ of the resonant field. Panel (b): nonzero damping; $\Gamma^{(3)}=0.1$ and $\Gamma^{(1)}=\Gamma^{(2)}=0$. In the dashed region, the spin has two coexisting stable equilibria in the rotating frame.

Then, from Eq. (15) for the merging saddle and node,

$$\mathcal{T}=-4\ \mathrm{sgn}(\mu)\sqrt{1-|f|^{2/3}}(4\Gamma^{(1)}(1-2|f|^{2/3}) +4\Gamma^{(2)}|f|^{2/3}+\Gamma^{(3)}). \tag{17}$$

If damping $\propto\Gamma^{(1)}$ is weak, the node is stable for $\mu>0$ and unstable for $\mu<0$. On the other hand, if $\Gamma^{(1)}$ is not small compared to $\Gamma^{(2,3)}$, the stability depends on the value of f.

The most significant difference between the saddle-node bifurcation curve and the Stoner–Wohlfarth astroid is that the bifurcation curve consists of two curvilinear triangles, that is, the astroid is "split" [see Figs. 2(b) and 5]. This is also the case for a modulated magnetic nanoparticle.[16] The triangles are obtained from Eqs. (13) and (16). After some algebra, we find that the "bases" of the bifurcation triangles are given by

$$f_B\approx\pm\Gamma_d(\mu)(1-\mu^2)^{1/2} \tag{18}$$

to leading order in Γ_d. This expression applies not too close to the vertices of the triangles. We note, however, that Eq. (18) gives the exact bifurcational value of f_B for $\mu=0$ and arbitrary $\Gamma_d(0)$.

The shape of the gap between the upper and lower curvilinear bifurcation triangles depends on the damping mechanism. In particular, the damping $\propto\Gamma^{(1)}$ does not contribute to the gap for small $|\mu|$ (cf. Fig. 5), whereas the damping $\propto\Gamma^{(2)}$ does not contribute to the gap at small $1-|\mu|$. The damping-induced change of the sides of the triangles compared to the astroid is quadratic in Γ_d far from the small-f range.

The positions of the small-f vertices of the bifurcation triangles f_C,μ_C for small damping can be found from Eq. (13) and the condition that Eq. (16) has a degenerate root, which gives

$$\mu_C\approx\pm[1-\sqrt{3}(-\Gamma_d^2+\mathcal{T}\Gamma_d)^{1/2}],$$

$$f_C\approx\pm(64/27)^{1/4}\Gamma_d^{3/4}(\Gamma_d+(1/2)\mathcal{T})^{1/2}(-\Gamma_d+\mathcal{T})^{1/4},$$

where Γ_d and $\mathcal{T}$ are calculated for $s_z=1$.

C. Periodic states and Hopf bifurcations

An important property of the modulated classical spin is the possibility to have periodic states in the rotating frame.

Such states result from Hopf bifurcations in which a stationary state transforms into a limit cycle.[22] A Hopf bifurcation occurs if

$$\mathcal{T}=0, \quad \mathcal{D}>0$$

in the stationary state. Besides the special case $s_z=0$ discussed in Sec. IV, the corresponding stationary state is at $s_z=s_{zH}$, where

$$s_{zH}=\frac{1}{2}\alpha\left(\frac{4\Gamma^{(1)}-4\Gamma^{(2)}-\Gamma^{(3)}}{2\Gamma^{(1)}-\Gamma^{(2)}}\right)^{1/2},$$

$$\alpha=\pm 1, \quad \Gamma^{(1)}\geq\Gamma^{(2)}+\frac{1}{4}\Gamma^{(3)}. \tag{19}$$

The inequality on the scaled decay rates $\Gamma^{(1)-(3)}$ follows from the condition $0\leq(s_z^2)_H\leq 1$.

On the Hopf bifurcation lines, the field f_H as a function of the reduced detuning μ is given by a particularly simple expression for weak damping. In this case, from the second equation of Eq. (13), the phase ϕ_H for the bifurcating stationary state is close to either 0 or π with the additional constraint $\partial_{s_z}^2 g\partial_\phi^2 g>0$. Then, from the first equation of Eq. (13) and Eq. (19), we find that Hopf bifurcation curves are straight lines on the (μ,f) plane in the limit of vanishingly small damping,

$$f_H=\pm[1-s_{zH}^2]^{1/2}[1+\mu s_{zH}^{-1}], \tag{20}$$

$$|f_H|\geq[1-s_{zH}^2]^{3/2} \quad \text{or} \quad |\mu|\geq|s_{zH}|. \tag{21}$$

The structure of these lines is seen in Fig. 5 below. They end on the saddle-node bifurcation curves and are tangent to these curves at the end points. A detailed analysis is presented in Sec. VI.

IV. HAMILTONIAN-LIKE MOTION AT EXACT RESONANCE

The spin dynamics (12) displays an unusual and unexpected behavior, where the modulation frequency ω_F coincides with the Larmor frequency ω_0, in which case $\mu=0$. This is a consequence of the symmetry of the quasienergy and the dissipation operator. In a certain range of dynamical variables ϕ,s_z, the spin behaves as a dissipationless system even though dissipation is present. This behavior is seen in the pattern of phase trajectories of the spin. An example of the pattern is shown in Fig. 1(c) for the case $\Gamma^{(2)}=\Gamma^{(3)}=0$, but the behavior is not limited to this case. As seen from Fig. 1(c), phase trajectories form closed loops, typical for Hamiltonian systems.

We start the analysis with the case of $|f|$ lying inside the bifurcation triangles on the (μ,f) plane, i.e., for $\Gamma_d(0)<|f|<[1+\Gamma_d^2(0)]^{1/2}$ [the upper bound on $|f|$ for $\mu=0$ can be easily obtained from Eqs. (13) and (16)]. Here, the spin has four stationary states. For small $|\mu|$, two of them have small $|s_z|$, $s_z\approx-\mu/(1-f\cos\phi)$, where $\sin\phi\approx-\Gamma_d(0)/f$. One of these states is a saddle point $\{\phi\approx-\arcsin[\Gamma_d(0)/f]\}$ and the other is a focus $\{\phi\approx\pi+\arcsin[\Gamma_d(0)/f]\}$.

For $\mu=0$, there occurs a global bifurcation, a homoclinic saddle-saddle bifurcation (saddle loop[22]) where the separatrix coming out from the saddle goes back into it, forming a homoclinic orbit. Simultaneously, the focus inside the loop becomes a center, $\mathcal{T}=0$ for $s_z=0$. All trajectories inside the homoclinic orbit are closed loops. The pattern persists throughout a broad region of f.

We show how the homoclinic bifurcation occurs and a Hamiltonian-like region in the phase space emerges first for weak damping. For $\mu=0$, the quasienergy g corresponds to the Hamiltonian of a spin with anisotropy energy $\propto S_z^2$, which is in a transverse field $\propto f$. Such spin in quantum mechanics has special symmetry, it can be mapped onto a particle in a symmetric potential.[9,10] Classical orbits $g=$const that surround the center $(s_z=0,\phi=\pi)$ are closed loops on the (ϕ,s_z) plane. They are symmetric with respect to the replacement

$$s_z\rightarrow -s_z, \quad \phi\rightarrow\phi, \tag{22}$$

which leads to $\dot{\phi}\rightarrow-\dot{\phi}$ and $\dot{s}_z\rightarrow\dot{s}_z$.

Weak damping would normally cause drift of quasienergy. The drift velocity averaged over the period $\tau_p(g)$ of motion along the orbit is

$$\langle\dot{g}\rangle=-\tau_p^{-1}\int_0^{\tau_p}d\tau\partial_{s_z}g\Gamma_d(s_z)(1-s_z^2). \tag{23}$$

From the symmetry (22) and the relation $\Gamma_d(s_z)=\Gamma_d(-s_z)$, we have $\langle\dot{g}\rangle=0$ on a closed orbit for $\mu=0$. Therefore, a closed orbit remains closed to first order in Γ_d. Of course, for open orbits, where ϕ is incremented by 2π over a period, $\langle\dot{g}\rangle\neq 0$. These orbits become spirals in the presence of damping.

Spirals and closed orbits should be separated by a separatrix, which must be a closed orbit itself. Since the separatrix must start and end at the saddle point, we understand that at $\mu=0$, for small Γ_d there occurs a saddle-saddle homoclinic bifurcation.

The topology discussed above persists as Γ_d increases. The symmetry (22) is not broken by Γ_d. Indeed, from equations of motion (13), any orbit that crosses $s_z=0$ twice per period for $\mu=0$ has the property (22) and therefore is closed. The closed orbits surround the center $s_z=0,\phi=\pi+\arcsin(\Gamma_d(0)/f)$ and fill out the whole interior of the separatrix loop.

The Hamiltonian-like behavior is displayed also for $\mu=0$ and f lying outside the bifurcation triangles. Here, the system has two stationary states, both with $s_z=0$ but with different ϕ. From Eq. (15), for both of them, $\mathcal{T}$ changes sign as μ goes through zero. Because there is no saddle point, there is no separatrix either: trajectories spiral toward or away from stationary states and possibly limit cycles. It follows from the arguments above that for $\mu=0$, all trajectories become closed orbits. This is confirmed by numerical calculations for different relaxation mechanisms.

It is convenient to analyze the overall dynamics of the spin system for $\mu\neq 0$ separately for the cases where the system does or does not have stable periodic states in the rotat-

ing frame. In turn, this is determined by the interrelation between the damping parameters [cf. Eq. (19)]. Such analysis is carried out in Secs. V and VI.

V. SPIN DYNAMICS IN THE ABSENCE OF LIMIT CYCLES

We start with the case where the system does not have limit cycles. It corresponds to the situation where the damping parameter $\Gamma^{(1)}$ is comparatively small and the interrelation between the damping parameters (19) does not hold. To simplify, the analysis we set $\Gamma^{(1)}=\Gamma^{(2)}=0$, i.e., we assume that the coupling to the bath is linear in the spin operators and is described by the interaction Hamiltonian $H_i^{(3)}$. The qualitative results of this section apply also for nonzero $\Gamma^{(1)},\Gamma^{(2)}$ as long as $\Gamma^{(3)}+4\Gamma^{(2)}>4\Gamma^{(1)}$. The bifurcation diagram for this case is shown in Fig. 2.

From the form of the function $\mathcal{T}$[Eq. (15)], it follows that the damping $\propto\Gamma^{(3)}$ transforms centers of conservative motion with $s_z>0$ into unstable foci (repellers), whereas the centers with $s_z<0$ are transformed into stable foci (attractors). Therefore, for $\mu<0$, the spin has one stable state. It also has one stable state in the unshaded region $\mu>0$ on the μ,f plane (outside the bifurcation triangles in Fig. 2). Inside the shaded regions within the triangles, the spin has two coexisting stable states.

Examples of the phase portrait are shown in Fig. 1. As expected, for weak damping, the system has a stable and an unstable focus outside the bifurcation triangles [Fig. 1(a)]. In the shaded region inside the triangle, it has two stable foci, an unstable focus, and a saddle point [Fig. 1(d)]. In the unshaded region inside the triangle, there is one stable and two unstable foci [Fig. 1(b)] [the values of μ in Figs. 1(b) and 1(d) differ just by the sign].

A. Hysteresis of spin response in the absence of limit cycles

The presence of two coexisting stable states leads to hysteresis of the spin response to the external field. Such hysteresis with varying dimensionless parameter μ, which is proportional to the detuning of the field frequency, is shown in Fig. 3. For large negative μ, the system has one stable state with negative s_z [cf. Fig. 1(a)]. As μ increases, the system stays on the corresponding branch (the lowest solid line in Fig. 3) until the stable state merges with the saddle point (the saddle-node bifurcation). This happens for $\mu>0$ as μ goes through the bifurcation triangle and reaches its large-μ boundary. As μ further increases, the system switches to the branch with larger s_z and then moves along this branch. If μ decreases starting with large values where the system has only one stable state, the switching to the second branch occurs for $\mu=0$.

The hysteresis pattern in Fig. 3 differs qualitatively from the standard S-shape characteristic. This is the case for any f lying between the minimum and maximum of the bifurcation triangle for $\mu=0$, i.e., for $2\Gamma^{(3)}<|f|<(1+4\Gamma^{(3)2})^{1/2}$. It is a consequence of the symmetry of the system that leads to the occurrence of a bifurcation at $\mu=0$. This bifurcation is not of a saddle-node type, whereas a most frequently considered

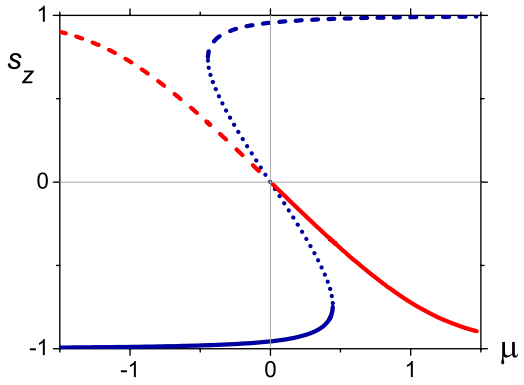

FIG. 3. (Color online) Hysteresis of spin response in the absence of periodic states in the rotating frame. The data refer to scaled decay rates $\Gamma^{(1)}=\Gamma^{(2)}=0$ and $\Gamma^{(3)}=0.1$ and scaled modulation amplitude $f=0.3$. The solid and dashed lines show, respectively, stable and unstable stationary states; the dotted line shows the saddle point.

S-shape hysteresis curve arises if both bifurcations are of the saddle-node type. In our case, for $\mu=0$, the branch which is stable in the range of large positive μ (the upper stable branch in Fig. 3) becomes unstable as a result of the motion becoming Hamiltonian-like. The value of s_z on this branch for $\mu=0$ is $s_z=0$; it coincides with the value of s_z at the saddle, but the values of s_x are different. Therefore, when s_z is plotted as a function of μ the branch, which is stable for large positive μ, crosses the branch that corresponds to the saddle point. For negative μ, the branch, which is stable for large positive μ, becomes unstable [cf. Fig. 1]. For positive μ, the system has also a branch of unstable stationary states shown by the dashed line. As μ decreases and reaches the negative-μ side of the bifurcation triangle, this branch merges with the branch of saddle states, as seen in Fig. 3.

The spin components display hysteresis also if the shaded area of the bifurcation triangle in Fig. 2(b) is crossed in a different way, for example, by varying f. If the crossing occurs so that the line $\mu=0$ is not crossed, the hysteresis curves have a standard S shape. We note that the associated hysteresis of s_x,s_y corresponds to hysteresis of amplitude and phase of forced vibrations of the spin.

B. Interbranch switching without hysteresis

The occurrence of Hamiltonian dynamics for $\mu=0$ leads to an interesting and unusual behavior of the system even outside the bifurcation triangles, i.e., in the region where the system has only one stable state. In the small damping limit and for $|f|>1$ and $|\mu|\ll 1$, the stationary states are at $\phi=0$ and $\phi=\pi$, with $s_z=\mu/(f\cos\phi-1)$. The stable state is the one with $s_z<0$, whereas the one with $s_z>0$ is unstable. As μ goes through zero, the states with $\phi=0$ and $\phi=\pi$ interchange stability. This means that $s_x\approx\cos\phi$ jumps between -1 and 1. Such switching is seen in Fig. 4.

VI. SPIN DYNAMICS IN THE PRESENCE OF LIMIT CYCLES

The classical dynamics of the spin changes significantly if the spin has stable periodic states in the rotating frame. This

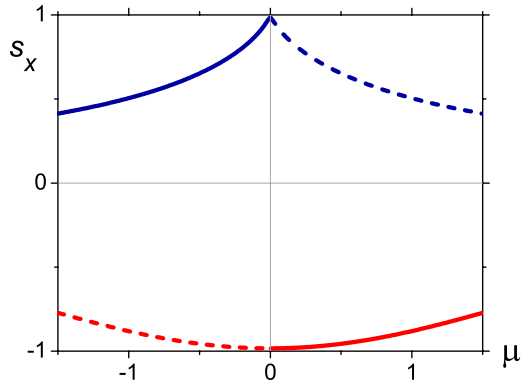

FIG. 4. (Color online) Frequency dependence of the transverse spin component for field amplitudes f where the system has one stable state. The solid and dashed lines show the stable and unstable values of s_x in the rotating frame. The data refer to $\Gamma^{(1)}=\Gamma^{(2)}=0$, $\Gamma^{(3)}=0.1$, and $f=1.1$. As the scaled frequency detuning μ goes through $\mu=0$, the spin component s_x changes sign.

occurs where condition (19) on the damping parameters is met. The features of the dynamics can be understood by setting $\Gamma^{(2)}=\Gamma^{(3)}=0$ and $\Gamma^{(1)}>0$, i.e., by assuming that damping is due primarily to coupling to a bath $H_i^{(1)}$, which is quadratic in spin components, with elementary scattering processes corresponding to transitions between neighboring Zeeman levels. This model is of substantial interest for single-molecule magnets.[18,21]

The saddle-node bifurcation curves for weak damping $\propto\Gamma^{(1)}$ are shown in Fig. 5. Inside the curvilinear triangles, the spin has four stationary states, whereas outside the triangles it has two stationary states. In contrast to the case of damping $\propto\Gamma^{(3)}$ shown in Fig. 2, in the present case, the bases of the triangles touch at $\mu=0$. From Eq. (17), one of the states emerging on the sides of the triangles is stable for $\mu>0, |f|<2^{-3/2}$ and is unstable otherwise; note that the stability changes in the middle of the bifurcation curves.

The occurrence of periodic oscillations of the spin is associated with Hopf bifurcations. In the case $\Gamma^{(2)}=\Gamma^{(3)}=0$, from Eq. (19), the Hopf bifurcational values of s_z are s_{zH}

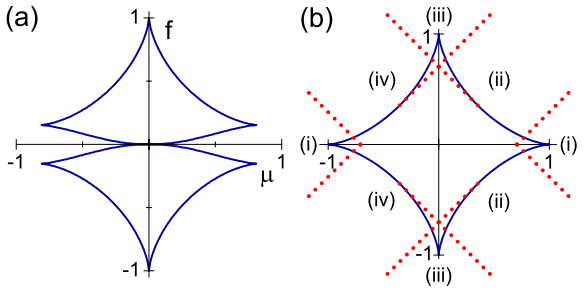

FIG. 5. (Color online). (a) Saddle-node bifurcation lines for scaled decay rates $\Gamma^{(1)}=0.05$ and $\Gamma^{(2)}=\Gamma^{(3)}=0$. (b) Saddle-node (solid lines) and Hopf bifurcation (dotted lines) in the limit $\Gamma^{(2)}=\Gamma^{(3)}=0$ and $\Gamma^{(1)}\to 0$. Not too close to the astroid (see Sec. VI B) for weak damping the system has the following states: (i) a stable and an unstable focus, (ii) two unstable foci and a stable limit cycle, (iii) a stable and an unstable focus and a stable and an unstable limit cycle, and (iv) two stable foci and an unstable limit cycle.

$=\pm 1/\sqrt{2}$. Therefore, Eq. (20) for the Hopf bifurcation lines for weak damping takes a simple form

$$f_H = 2^{-1/2} \pm \mu, \quad f_H \notin (0, 2^{-3/2}),$$

$$f_H = -2^{-1/2} \pm \mu, \quad f_H \notin (-2^{-3/2}, 0). \tag{24}$$

These lines are shown in Fig. 5(b). For $|f|\sim 1$ and far from the end points of the bifurcation lines, the typical frequency of the emerging oscillations is ~ 1 in dimensionless units or $\sim DS/\hbar$ in dimensional units.

A. Phase portrait far from the astroid

Evolution of the spin phase portrait with varying parameters far away from the astroid, $|\mu|\gg 1$, can be understood by looking at what happens as the Hopf bifurcation curves are crossed, for example, if f is varied. The question is on which side of the bifurcation curve there emerges a limit cycle and whether this cycle is stable or unstable. This question can be answered by looking at two characteristics. One is stability of the stationary state for f close to the bifurcational value f_H. The stability depends on the sign of $\mathcal{T}$ for small $f-f_H$ (note that $\mathcal{T}$ changes sign for $f=f_H$). The other characteristic is the sign of the quasienergy drift velocity $\langle\dot{g}\rangle$ for $f=f_H$ and for g close to its bifurcational value g_H at the stationary state. It is given by Eq. (23) [note that, generally, $\langle\dot{g}\rangle\propto(g-g_H)^2$ for $f=f_H$].

We write the value of s_z at the Hopf bifurcation point as $s_{zH}=\alpha/\sqrt{2}$, where $\alpha=\pm 1$ [cf. Eq. (19)]. The bifurcational value of the field (24) is $f_H=\pm(2^{-1/2}+\alpha\mu)\cos\phi_H$, where ϕ_H is the phase of the bifurcating stationary state. Linearizing Eq. (15) in s_z-s_{zH} and using the explicit form of the determinant $\mathcal{D}$, one can show that, for small $f-f_H$, in a stationary state $\mathrm{sgn}[\mathcal{T}/(f-f_H)]=-\mathrm{sgn}[\alpha f_H]$. Then,

$$\mathrm{sgn}\,\mathcal{T} = -(\alpha\,\mathrm{sgn}\,f_H)\mathrm{sgn}(f-f_H). \tag{25}$$

The analysis of the quasienergy drift velocity near a Hopf bifurcation point is done in the Appendix. It follows from Eqs. (A1) and (A2) that

$$\langle\dot{g}\rangle = C\alpha\Gamma^{(1)}(g-g_H)^2(\beta|f_H|-\sqrt{2}),$$

$$\mathrm{sgn}[\langle\dot{g}\rangle/(g-g_H)] = \alpha\beta\,\mathrm{sgn}(\beta|f_H|-\sqrt{2}), \tag{26}$$

where $C>0$ is a constant and $\beta=\mathrm{sgn}(f_H\cos\phi_H)\equiv\mathrm{sgn}(2^{-1/2}+\alpha\mu)=\pm 1$ [μ is related to f_H by Eq. (24); the sign of $g-g_H$ depends on whether g has a local maximum or minimum at the stationary state].

The sign of $\langle\dot{g}\rangle/(g-g_H)$ shows whether g approaches g_H as a result of damping or moves away from g_H. If $\mathrm{sgn}[\langle\dot{g}\rangle(g-g_H)]<0$, the vicinity of the stationary state and the nascent limit cycle attracts phase trajectories. Therefore, at a Hopf bifurcation, a stable focus becomes unstable and a stable limit cycle emerges. On the other hand, if $\mathrm{sgn}[\langle\dot{g}\rangle(g-g_H)]>0$, at a Hopf bifurcation an unstable focus transforms into a stable one and an unstable limit cycle emerges.

The above argument allows one to tell on which side of the bifurcation line there emerges a limit cycle since the sign

of $\langle \dot{g} \rangle / (g - g_H)$ does not change as f crosses f_H, whereas the sign of $\mathcal{T}$ does. The limit cycle is on the side of $f - f_H$, where $\langle \dot{g} \rangle / (g - g_H)$ and $\mathcal{T}$ have opposite signs. Equations (25) and (26) determine also whether the nascent limit cycle is stable.

We are now in a position to describe which states exist far from the astroid in different sectors (i)–(iv) in Fig. 5(b). For small $|f|$ and large $|\mu|$, region (i) in Fig. 5(b), the system is close to a spin in thermal equilibrium, it has one stable and one unstable stationary state. We now start changing f staying on the side of large positive μ. When f crosses one of the bifurcation curves $f_H = \pm(2^{-1/2} - \mu)$, the system goes to one of the regions (ii) in Fig. 5(b). It follows from the analysis above that on both bifurcation curves, $\alpha = \beta = -1$. Therefore, from Eqs. (25) and (26), when one of these curves is crossed as $|f|$ increases, there emerges a stable limit cycle, and the stable focus becomes unstable. As $|f|$ further increases, it crosses the bifurcation curves $\pm(2^{-1/2} + \mu)$ and the system goes to one of the regions (iii) in Fig. 5(b) (we assume that the crossing occurs in the region $|f_H| > 2^{1/2}$). One can see that on these bifurcation curves, $\alpha = \beta = 1$. Therefore, from Eqs. (25) and (26), when they are crossed with increasing $|f|$, there emerges an unstable limit cycle and the unstable focus becomes stable.

We now start from the range of large negative μ and small $|f|$. As we increase $|f|$ and cross the bifurcation curves $f_H = \pm(\mu + 2^{-1/2})$, the system goes from region (i) to one of the regions (iv) in Fig. 5(b). From Eqs. (25) and (26), in this case, an unstable focus goes over into a stable focus and an unstable limit cycle emerges. Further crossing into one of the regions (iii) with increasing $|f|$ leads to a transformation of a stable focus into an unstable focus and an onset of a stable limit cycle. These arguments were used to establish the nomenclature of states in regions (i)–(iv) in Fig. 5(b). They agree with the results of direct numerical calculations.

B. Other bifurcations of limit cycles

1. Merging of stable and unstable limit cycles

The number of periodic states in the rotating frame may change not only through Hopf bifurcations but also through other bifurcations, where the radius of the bifurcating limit cycle does not go to zero. The simplest is a bifurcation where a stable limit cycle merges with an unstable limit cycle (saddle-node bifurcation of limit cycles). The onset of such bifurcations is clear already from Eq. (26). Indeed, at a Hopf bifurcation point, the equation for the period-averaged quasienergy has a form $\langle \dot{g} \rangle = c(g - g_H)^2 + \cdots$, with $c \propto \beta |f_H| - \sqrt{2}$. For $|f_H| = \sqrt{2}$ on the bifurcation curves (24) with $\beta = 1$ [the top and bottom dotted lines in Fig. 5(b)], the coefficient $c = 0$. This is a generalized Hopf bifurcation[22] (see Fig. 6).

At the generalized Hopf bifurcation, in phase space (ϕ, s_z) a stationary state merges simultaneously with a stable and an unstable limit cycle. In parameter space (μ, f), the Hopf bifurcation curve coalesces with the curve where stable and unstable limit cycles are merging, and the latter curve ends. The bifurcation curves are tangent; the distance between them scales as a square of the distance to the end point $\beta |f_H| = \sqrt{2}$ close to this point. This is seen in Fig. 6. In the comparatively narrow region between the Hopf bifurcation curve and the curve on which limit cycles merge, the system has three limit cycles. One of them disappears on the Hopf bifurcation curve so that in region (iii) in Fig. 5(b), there are two limit cycles, and deeper in regions (ii) and (iv), there is one limit cycle. On its opposite end, the curve of merging limit cycles coalesces with the saddle-loop bifurcation curve.

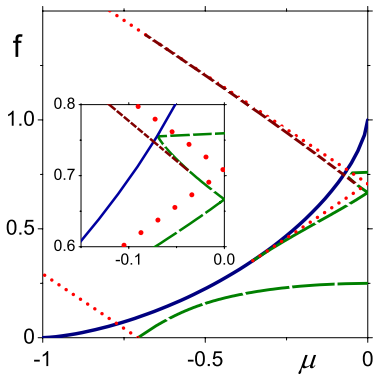

FIG. 6. (Color online) Bifurcation diagram in the limit $\Gamma^{(1)} \to 0$. The diagram is symmetric with respect to $\mu = 0$ and $f = 0$ axes, and therefore, only the quadrant $f \geq 0$ and $\mu \leq 0$ is shown. Saddle-node, Hopf, and saddle-loop bifurcation curves are shown by the solid, dotted, and long-dashed lines, respectively, whereas the short-dash line shows the curve on which stable and unstable limit cycles merge.

2. Saddle loops

Spin dynamics for damping $\propto \Gamma^{(1)}$ is characterized also by global bifurcations of the saddle-saddle (saddle-loop) type. This is clear already from the analysis of the end points of the Hopf bifurcation curves. These points lie on the curves of saddle-node bifurcations. The corresponding equilibrium point $(\dot{s}_z = \dot{\phi} = 0)$ has double-zero eigenvalue. The behavior of the system near this point is well known.[22] The Hopf bifurcation curve is tangent to the saddle-node bifurcation curve at the end point. In addition, there is a saddle-loop bifurcation curve coming out of the same end point and also tangent to the saddle-node bifurcation curve at this point. At a saddle-loop bifurcation, the system has a homoclinic trajectory that starts and ends at the saddle point.

The structure of vicinities of the end points of the Hopf bifurcation curves is shown in Figs. 6 and 7 for the curves ending on the sides and the bases of the saddle-node bifurcation triangles, respectively. Note that the Hopf bifurcation curves that crossed at $f = 0$ in the limit $\Gamma^{(1)} \to 0$ are separated for finite $\Gamma^{(1)}$. They end on the saddle-node bifurcation curves. We have found numerically a fairly complicated pattern of saddle-loop bifurcation curves, as seen in Fig. 6. The full analysis of this pattern is beyond the scope of this paper.

C. Hysteresis of spin response in the presence of limit cycles

The coexistence of stable stationary states and stable limit cycles in the rotating frame leads to hysteresis of the response of a spin when the modulating field parameters are

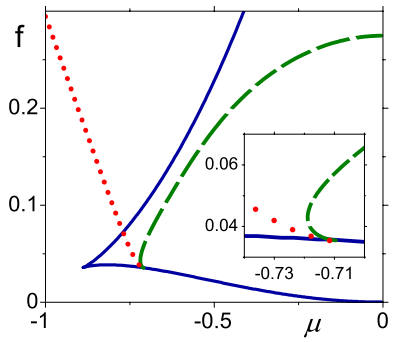

FIG. 7. (Color online) Bifurcation diagram near the end point of the Hopf bifurcation line, which in the limit $\Gamma^{(1)}\to 0$ has the form $f_H=-\mu-2^{-1/2}$. For nonzero $\Gamma^{(1)}$, this bifurcation line ends on the saddle-node bifurcation line (18). The plot refers to $\Gamma^{(1)}=0.0125$. The inset shows a close vicinity of the end point. Hopf, saddle-node, and saddle loop bifurcation curves are shown by dotted, solid, and long-dashed lines, respectively. Other Hopf bifurcation curves that go to $f_H=0$ for $\Gamma^{(1)}\to 0$ display a similar behavior near their end points.

slowly varied. Examples of such hysteresis with varying scaled frequency detuning μ and the characteristic phase portraits are shown in Fig. 8.

The hysteretic behavior is unusual. This is a consequence of the feature of the spin dynamics for $\mu=0$ where either all

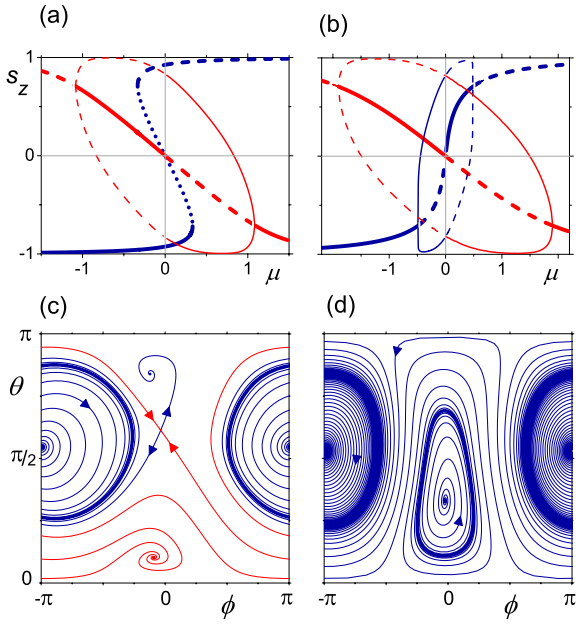

FIG. 8. (Color online). Panels (a) and (b): hysteresis of spin response with varying scaled detuning of the modulating field frequency μ. In (a) $f=0.4$ so that μ goes through the curvilinear bifurcation triangle in Fig. 5. In (b) $f=1.2$, it lies above the triangles. The bold solid, dashed, and dotted lines show stable, unstable, and saddle stationary states, respectively. Pairs of thin solid and dashed lines show, respectively, the boundaries (with respect to s_z) of stable and unstable limit cycles. Panels (c) and (d): phase portraits for $\mu=0.2$. In (c) and (d), $f=0.4$ and 1.2, respectively. The arrows show the direction of motion along the trajectories. The data refer to $\Gamma^{(1)}=0.05$.

phase trajectories are closed loops (for f outside the curvilinear saddle-node bifurcation triangles in Fig. 5) or all trajectories in a part of the phase plane are closed loops (for f inside the triangles in Fig. 5). As a result, two or more states (stationary or periodic) simultaneously change stability as μ goes through 0. This leads to an ambiguity of switching, a "Buridan's ass" type situation. Where a stable branch looses stability for $\mu=0$, the system has more than one stable state to switch to. Also, in contrast to the situation of Sec. V where the system had no limit cycles, hysteresis emerges whether the varying field parameter does or does not cross the saddle-node bifurcation lines.

Figures 8(a) and 8(b) show the behavior of the system with varying μ for f inside and outside the saddle-node bifurcation triangles, respectively. It should be noted that we chose f in Fig. 8(a) so that the saddle-loop bifurcation line is not encountered, which provides an insight into the most basic features of the hysteresis. In addition, in Fig. 8(b) we do not show an extremely narrow region near Hopf bifurcation lines $\mu\approx\pm(f-2^{-1/2})$, where the system has small-radii stable and unstable cycles which merge on the short-dash bifurcation line in Fig. 6.

In Fig. 8(a), for large negative μ, the system has one stable state (with negative s_z). As μ increases, this state disappears via a saddle-node bifurcation and the system switches to a stable limit cycle. For chosen $f=0.4$, this happens for $\mu\approx 0.33$. With further increase in μ, the limit cycle shrinks and ultimately disappears via a Hopf bifurcation, and then the stationary state inside the cycle becomes stable.

On the other hand, if we start in Fig. 8(a) from large positive μ and decrease μ, the stable stationary state via a supercritical Hopf bifurcation becomes a stable limit cycle. The cycle looses stability at $\mu=0$, and as μ becomes negative, the system can switch either to the stable stationary state inside the cycle (with $s_z\to+0$ for $\mu\to-0$) or to the stable stationary state outside the cycle with negative s_z. The stable state with $s_z\to+0$ for $\mu\to-0$ ultimately looses stability with decreasing μ via a Hopf bifurcation (at $\mu\approx-f-2^{-1/2}$, for small damping, cf. Fig. 5). If the system is in this state, it switches to the stable equilibrium with negative s_z.

A typical phase portrait for $f=0.4, 0<\mu<0.33$ is shown in Fig. 8(c). It gives an insight into the behavior described above. The system has a stable limit cycle with an unstable focus inside and with stable and unstable equilibria and a saddle point outside the limit cycle. For $\mu=0$, the system has a homoclinic saddle connection, and all trajectories inside the homoclinic trajectory are closed loops [cf. Fig. 1(c)].

In Fig. 8(b), for large negative μ, the system also has one stable state (with negative s_z). As μ increases, this state looses stability via a Hopf bifurcation (at $\mu\approx-f+2^{-1/2}$, for small damping). The emerging state of stable oscillations looses stability for $\mu=0$. For larger μ, the system switches either to the stationary state inside the limit cycle (with $s_z\to+0$ for $\mu\to+0$) or to another stable periodic state. The coexistence of stable and unstable limit cycles with stationary states inside of them is seen in Fig. 8(d).

As μ becomes positive and further increases, the stable stationary state inside the unstable cycle looses stability via a Hopf bifurcation, and the system switches to the periodic

state corresponding to the stable limit cycle in Fig. 8(d). For still larger μ ($\mu \approx f+2^{-1/2}$, for weak damping), this state experiences a Hopf bifurcation and becomes a stable stationary state. The behavior with μ decreasing from large positive values can be understood from Fig. 8 in a similar way.

VII. CONCLUSIONS

We have developed a microscopic theory of a resonantly modulated large spin in a strong static magnetic field and studied the spin dynamics in the classical limit. We have taken into account relaxation processes important for large-spin systems of current interest. They correspond to transitions between neighboring and next neighboring Zeeman levels with emission or absorption of excitations of a bosonic thermal bath, in particular, phonons or magnons. The classical spin dynamics depends significantly on the interrelation between the rates of different relaxation processes. Generally, it is not described by the Landau–Lifshitz equation for magnetization in a ferromagnet, although one of the coupling mechanisms that we discuss leads, in the rotating frame, to the same friction force as what follows from the Landau–Lifshitz equation.

We found that the spin dynamics has special symmetry at exact resonance, where the modulation frequency is equal to the Larmor frequency, $\omega_F=\omega_0$. This symmetry leads to a Hamiltonian-like behavior even in the presence of dissipation. In the rotating frame, phase trajectories of the spin form closed loops in a part of or on the whole phase plane. Therefore, when ω_F goes through ω_0 several states can change stability at a time.

The simultaneous stability change leads to unusual observable features. Where the system has only one stable state for a given parameter value, i.e., there is no hysteresis, as ω_F goes through ω_0 there occurs switching between different states. It leads to an abrupt change of the resonant transverse magnetization.

We found the conditions where the spin has more than one stable state in the rotating frame. Multistability leads to magnetization hysteresis and interbranch switching with varying parameters of the modulating field. The switching behavior becomes complicated where several stable states coexist for ω_F close but not equal to ω_0. Here, if the occupied stable state looses stability with varying ω_F for $\omega_F=\omega_0$, the state into which the system will switch is determined by fluctuations or by history if ω_F is changed comparatively fast.

If the fastest relaxation process is the transitions between neighboring Zeeman levels due to coupling quadratic in spin operators, along with stable stationary states in the rotating frame, the resonantly modulated spin can have stable periodic nonsinusoidal states (limit cycles on phase plane) with frequency $\propto DS/\hbar$, where D is the anisotropy energy. In the laboratory frame, these states correspond to oscillations of the transverse magnetization at combinations of the frequency in the rotating frame (and its overtones) and the driving frequency. In contrast, stationary states in the rotating frame correspond to transverse magnetization oscillations at the driving frequency in the laboratory frame.

Quantum fluctuations of the spin lead to phase diffusion of the classical periodic states in the rotating frame. As a result, classical oscillations lose coherence. The intensity of quantum fluctuations and the related relaxation rate depend on the value of S^{-1}. We have found[31] that the oscillations decohere comparatively fast even for $S=10$. Still, the classically stable vibrations lead to pronounced features of the full quantum spin dynamics.

The above analysis applies also to decay processes where a transition between spin Zeeman levels is accompanied by the emission or absorption of two phonons or magnons, or results from inelastic scattering of thermal phonons (magnons) by the spin. Such processes often play an important role in spin dynamics. We note that the results are not limited to linearly polarized radiation. It is easy to show that they apply for an arbitrary polarization as long as the radiation is close to resonance.

In conclusion, starting from a microscopic model, we have shown that the classical dynamics of a resonantly modulated large spin in a strong magnetic field displays several characteristic features. They include abrupt switching between magnetization branches with varying parameters of the modulating field even where there is no hysteresis, as well as the occurrence of hysteresis and an unusual pattern of hysteretic interbranch switching. These features are related to the Hamiltonian-like behavior of the dissipative spin for modulation frequency equal to the Larmor frequency (calculated in the neglect of the anisotropy energy). Along with forced vibrations at the modulation frequency, the transverse spin components can display incoherent vibrations at a combination of the modulation frequency and a slower frequency $\propto DS/\hbar$ and its overtones. They emerge if the fastest relaxation mechanism corresponds to transitions between neighboring Zeeman levels with the energy of coupling to a thermal bath quadratic in the spin operators.

ACKNOWLEDGMENTS

We are grateful to S. W. Shaw for the discussion of the bifurcation pattern and to J. Vidal for pointing to the analogy with the Lipkin–Meshkov–Glick model. This research was supported in part by the NSF through Grant No. PHY-0555346 and by the Institute for Quantum Sciences at MSU.

APPENDIX: ENERGY CHANGE NEAR A HOPF BIFURCATION

In this appendix, we outline the calculation of the relaxation of quasienergy g near a Hopf bifurcation point. For concreteness, we assume that $\Gamma^{(2)}=\Gamma^{(3)}=0$ and the only nonzero damping parameter is $\Gamma^{(1)}$. For small damping, a stationary state that experiences a bifurcation has phase ϕ_H close to either 0 or π, whereas $s_{zH}\approx \pm 2^{-1/2}$. The dynamics is characterized by two parameters, $\alpha=\mathrm{sgn}\, s_{zH}$ and $\beta=\mathrm{sgn}(f_H \cos\phi_H)$. The bifurcational value of the field for $\Gamma^{(1)}\to 0$ is $f_H=(2^{-1/2}+\alpha\mu)\cos\phi_H$ [cf. Eq. (24)].

At the bifurcating stationary state, the quasienergy is $g_H=g(\phi_H,s_{zH})$; it is easy to see that this is a local minimum of $g(\phi,s_z)$ for $\beta>0$ or a maximum for $\beta<0$. On phase plane

(ϕ, s_z), the constant-g trajectories close to the bifurcating stationary state rotate about this state clockwise for $\beta > 0$ and counterclockwise for $\beta < 0$. The angular frequency of this rotation is $\approx 2\pi/\tau_p(g_H) = \mathcal{D}^{1/2}$, where $\mathcal{D}$ is given by Eq. (14).

We now consider dissipation-induced drift over quasienergy $\langle \dot{g} \rangle$. It is determined by Eq. (23). Noting that $\partial_{s_z} g = \dot{\phi}$ and using the Stokes theorem, we can rewrite this equation as

$$\langle \dot{g} \rangle = \beta \tau_p^{-1}(g) \int d\phi ds_z \mathcal{T}, \tag{A1}$$

where the integral is taken over the interior of the constant-g orbit on the (ϕ, s_z) plane and $\mathcal{T} \equiv \mathcal{T}(s_z)$ is given by Eq. (15). At a Hopf bifurcation point $\mathcal{T} = 0$. Therefore, $\mathcal{T}(s_z)$ in Eq. (A1) must be expanded in $\delta s_z = s_z - s_{zH}$.

It is convenient to calculate integral (A1) by changing to integration over action-angle variables (I, ψ), which are canonically conjugate to (s_z, ϕ), with g as the effective Hamiltonian. The angle ψ gives the phase of oscillations with given quasienergy g. The action variable $I = (2\pi)^{-1} \oint s_z d\phi$ is related to g by the standard expression $dI/dg = \tau_p(g)/2\pi \approx \mathcal{D}^{-1/2}$; we note that I becomes negative for $\beta < 0$.

In evaluating expression (A1), it is further convenient to start with integrating $\mathcal{T}$ over ψ. The integral goes from 0 to 2π and gives the period average of $\mathcal{T}$ for a given $I \propto \delta g = g - g_H$ (integration over I corresponds to integration over δg).

If vibrations about (ϕ_H, s_{zH}) were harmonic, the lowest-order term in δs_z that would not average to zero on integration over ψ would be $(d^2\mathcal{T}/ds_z^2)(\delta s_z)^2/2 \propto |\delta g|$ (the derivative of $\mathcal{T}$ is calculated at the bifurcating stationary state). However, it is easy to see that the integral over ψ of the linear in δs_z term in $\mathcal{T}$ is also $\sim \delta g$ because of the nonlinearity of equations of motion. It can be calculated from equation $\dot{\phi} = \partial_{s_z} g$ by expanding the right-hand side to second order in $\delta s_z, \delta\phi$ and noting that $\bar{\dot{\phi}} = 0$, where the overline means averaging over ψ. This gives, after some algebra,

$$\langle \mathcal{T} \rangle = 64\Gamma^{(1)}\alpha(\delta g)(2^{3/2}\beta|f_H| - 1)^{-2}(\beta|f_H| - 2^{1/2}). \tag{A2}$$

This expression combined with Eq. (A1) shows how the energy relaxation rate depends on the field f_H. It is used in Sec. VI to establish the full bifurcation diagram.

[1] W. Wernsdorfer, Adv. Chem. Phys. **118**, 99 (2001).
[2] J. R. Friedman, in *Exploring the Quantum/Classical Frontier: Recent Advances in Macroscopic and Mesoscopic Quantum Phenomena*, edited by J. R. Friedman and S. Han (Nova Science, Huntington, NY, 2003), p. 179.
[3] D. Gatteschi, R. Sessoli, and J. Villain, *Molecular Nanomagnets* (Oxford University Press, New York, 2006).
[4] A. Sieber, G. Chaboussant, R. Bircher, C. Boskovic, H. U. Güdel, G. Christou, and H. Mutka, Phys. Rev. B **70**, 172413 (2004).
[5] M. Evangelisti *et al.*, Phys. Rev. Lett. **97**, 167202 (2006).
[6] M. N. Leuenberger and D. Loss, Phys. Rev. B **68**, 165317 (2003).
[7] C. Hicke and M. I. Dykman, Phys. Rev. B **76**, 054436 (2007).
[8] H. J. Lipkin, N. Meshkov, and A. J. Glick, Nucl. Phys. **62**, 188 (1965).
[9] V. V. Ulyanov and O. B. Zaslavskii, Phys. Rep. **216**, 179 (1992).
[10] D. A. Garanin, X. Martinez Hidalgo, and E. M. Chudnovsky, Phys. Rev. B **57**, 13639 (1998).
[11] P. Ribeiro, J. Vidal, and R. Mosseri, Phys. Rev. Lett. **99**, 050402 (2007).
[12] P. W. Anderson and H. Suhl, Phys. Rev. **100**, 1788 (1955).
[13] H. Suhl, J. Phys. Chem. Solids **1**, 209 (1957).
[14] G. V. Skrotskii and Y. I. Alimov, Sov. Phys. JETP **9**, 899 (1959).
[15] D. J. Seagle, S. H. Charap, and J. O. Artman, J. Appl. Phys. **55**, 2578 (1984).
[16] G. Bertotti, C. Serpico, and I. D. Mayergoyz, Phys. Rev. Lett. **86**, 724 (2001); A. Magni, G. Bertotti, C. Serpico, and I. D. Mayergoyz, J. Appl. Phys. **89**, 7451 (2001); G. Bertotti, I. Mayergoyz, and C. Serpico, *ibid.* **95**, 6598 (2004); C. Serpico, M. d'Aquino, G. Bertotti, and I. D. Mayergoyz, *ibid.* **95**, 7052 (2004).
[17] M. I. Dykman and M. A. Krivoglaz, *Soviet Physics Reviews* (Harwood, Academic, New York, 1984), Vol. 5, pp. 265–441.
[18] D. A. Garanin and E. M. Chudnovsky, Phys. Rev. B **56**, 11102 (1997).
[19] M. N. Leuenberger and D. Loss, Phys. Rev. B **61**, 1286 (2000).
[20] S. Bahr, K. Petukhov, V. Mosser, and W. Wernsdorfer, Phys. Rev. Lett. **99**, 147205 (2007).
[21] M. Bal, J. R. Friedman, W. Chen, M. T. Tuominen, C. C. Beedle, E. M. Rumberger, and D. N. Hendrickson, Europhys. Lett. **82**, 17005 (2008).
[22] J. Guckenheimer and P. Holmes, *Nonlinear Oscillators, Dynamical Systems and Bifurcations of Vector Fields* (Springer-Verlag, New York, 1997).
[23] A. L. Barra, A. Caneschi, D. Gatteschi, D. P. Goldberg, and R. Sessoli, J. Solid State Chem. **145**, 484 (1999); J. Kortus, T. Baruah, N. Bernstein, and M. R. Pederson, Phys. Rev. B **66**, 092403 (2002).
[24] J. Villain, F. Hartman-Boutron, R. Sessoli, and A. Rettori, Europhys. Lett. **27**, 159 (1994).
[25] R. L. Melcher, *Proceedings of the 1970 Ultrasonics Symposium* (IEEE, San Francisco, 1971), pp. 35–47.
[26] R. G. Shulman, B. J. Wyluda, and P. W. Anderson, Phys. Rev. **107**, 953 (1957).
[27] E. F. Taylor and N. Bloembergen, Phys. Rev. **113**, 431 (1959).
[28] Y. Izyumov, Proc. Phys. Soc. London **87**, 505 (1966).
[29] M. A. Krivoglaz and L. B. Kvashnina, Phys. Status Solidi **29**, 53 (1968).
[30] E. C. Stoner and E. P. Wohlfarth, Philos. Trans. R. Soc. London, Ser. A **240**, 599 (1948).
[31] C. Hicke and M. I. Dykman (unpublished).